

Optimizing Microscopic Magnetic Fields for Neuronal Stimulation.

Giorgio Bonmassar^a, John Gale^b and Wim Vanduffel^{a,c}

^a A. A. Martinos Center, Harvard Medical School, Massachusetts General Hospital, Charlestown, MA, USA

^b Department of Neuroscience, Cleveland Clinic, Cleveland, OH, USA.

^c Research Group Neurophysiology, KU Leuven, Leuven, Belgium.

Correspondence: G Bonmassar, A. A. Martinos Center, Harvard Medical School, Massachusetts General Hospital, Building 149

13th Street, Charlestown, MA 02129, USA. E-mail: gbonmassar@tmgh.harvard.edu

phone +1 617 726 0962, fax +1 617 726 74222.

Abstract. Micromagnetic stimulation (μ MS) has several advantages over electrical stimulation. First, μ MS does not require charge-balanced stimulation waveforms as in electrical stimulation.

In μ MS, neither sinks nor sources are present when a current is induced by the time-varying magnetic field, thus μ MS does not suffer from charge buildup as can occur with electrical stimulation. Second, magnetic stimulation via μ MS is capable of activating neurons with specific axonal orientations. We investigated the viability of stimulating neurons magnetically using microscopic coils having differing physical properties. As the size and core material permeability of the microcoils are altered, the strength of the current density fields generated by these microcoils will vary non-linearly. Finally the role of stimulation pulse-shape is explored, suggesting that triangular pulses with maximum slope or slew rate are ideal from the standpoint of energy efficiency. Energy efficiency may be achieved by a combination of coil optimizations, including: (a) pulse design, (b) energy harvesting, (c) high-permeability cores, (d) low Q-factor designs (e.g., spiral coils), (e) coil geometries of μ MS coil arrays. The resulting energy-efficient μ MS may allow for direct deployment on patients, who will benefit from reduced inflammation, MRI compatibility and enhanced stimulation capability offered by μ MS over traditional electrical stimulation.

Keywords: Eddy Currents, TMS, finite element method, microcoils, inductive stimulation.

1. Introduction

Microscopic magnetic stimulation (μ MS) uses submillimeter coils to stimulate local excitable tissue, as recently shown by activating retinal ganglion cells *in vitro* [1] and inferior colliculus neurons *in vivo* [2]. Neuronal stimulation is achieved by generating a dispersed magnetic flux density (e.g., 0.1 Tesla) in a focal region of tissue by discharging a time-varying current through a microscopic coil. If these coils are placed within or in close proximity to excitable tissue, they can induce a localized current gradient sufficient to activate the tissue. The time-varying signal applied to the coil may consist of currents of several amperes lasting up to tens of μ s.

There are several advantages to using μ MS over traditional electrical stimulation (ES) or transcranial magnetic stimulation (TMS). For example, with electrical stimulation, MRI examination of patients undergoing treatment with deep brain stimulation (DBS) can result in thermal injuries of the neural tissue due to presence of the stimulating

electrodes [3]. In these patients, Joule heating is generated by the combination of high RF current density J with the high impedance interface between the electrode and tissue [4]. With μ MS, the Joule heating, generated by currents densities J_i in the implant/tissue interface due to the presence of the implant (i.e., *antenna effect* [5]), may be greatly reduced by the use of a proper dielectric coating around the coil, such as thin film dielectrics [6] possessing the desired RF insulating characteristics [7]. Secondly, direct contact between metal and tissue in ES may cause inflammation and glial scarring around the stimulating electrode, increasing electrode impedance and stimulation threshold [8]. Although a number of mechanisms can induce the inflammatory process with common platinum electrodes (Pt), electrochemical stimulation-induced tissue trauma may involve irreversible O_2 and H_2 evolution, dissolution of Pt and reduction of dissolved O_2 at the electrode-tissue interface [9]. This reaction modifies the local pH and may generate inflammation in the surrounding tissue [10] that ultimately induces an immune reaction. This source of immune reaction can be avoided in μ MS by the use of biocompatible dielectrics [11]. Thirdly, unlike electrical stimulation any realistic pulse of magnetic stimulation does not result in charge accumulation in the tissue. Electrically charge-balanced pulse design is key to the safe electrical stimulation, thus

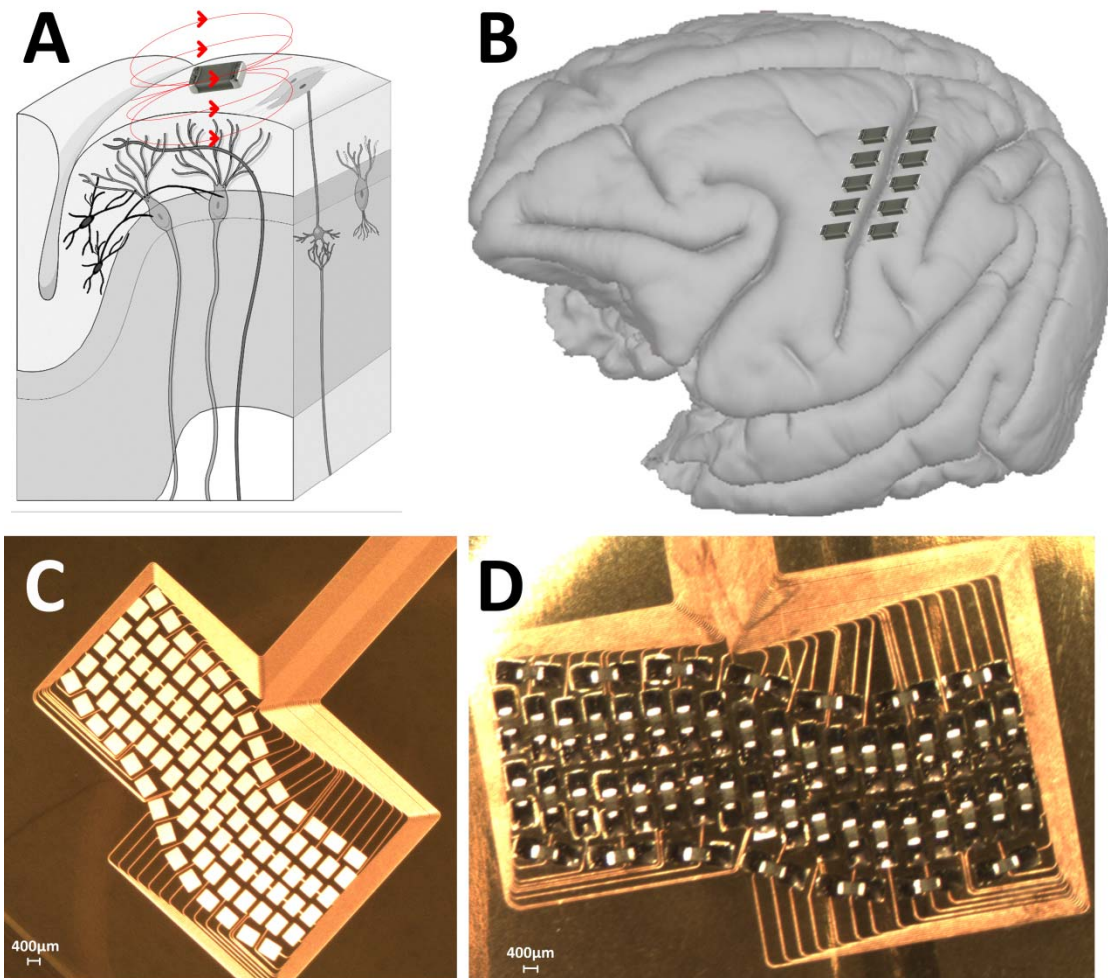


Fig. 1: Cortical stimulation by μ MS: (A) the magnetic field induced by the μ MS coil can excite cortical neurons when appropriate coil orientation, distance and pulse shapes are used, (B) design of a μ MS coils grid that follows the curvature of the somatomotor cortex of a nonhuman primate. (C) Layout of the actual FLEX circuit with 64 gold traces with $25\mu m$ width deposited with sputtering on $50\mu m$ thick Kapton substrate and (D) FLEX populated with 60 RF inductors type 0402 surface mount.

avoiding irreversible damage to excitable tissue from buildup of electrolysis byproducts [12]. Finally, the magnetic field has generally different penetration characteristics with respect to the electric field and hence the combination of both electric (**E**) and magnetic (**B**) fields can potentially improve neural stimulation.

Unlike TMS that requires bulky, custom-designed apparatus for charging and discharging large capacitors in order to generate currents in the kA range [13], μ MS can be driven by a small, class D amplifiers [1]. Furthermore, μ MS is capable of highly focal stimulation when placed in close proximity to the tissue (**Fig. 1**), even down to the level of neuronal cell body or axon, greatly increasing the gradient of the induced current density. According to the predictions of several neural models, it is the gradient of the electric field, rather than its strength, that is primarily responsible for neural activation [14].

Finally, sets of coils can be arranged into various spatial configurations, conveniently modifying the distribution of the magnetic flux (**Fig. 2**). For instance, the figure eight (**Fig. 2.A** with two [15] or more coils) configuration along with a simple circular element is the most commonly used coil type for TMS. This configuration provides a more focal and directed stimulus under the center of the coil [16]. In addition, the Helmholtz (**Fig. 2.B**) coil has been used for the stimulation of biological tissue and cells where a uniform magnetic field is desired [17]. Other configurations include the concentric dual toroid (**Fig. 2.C**) design used in advanced pulsed magnet design that allows different waveforms to be applied to each to coil to optimize magnetic flux, dampen mechanical vibration and reduce tensile radial stress [18]. The ability to steer the magnetic field with no physical movement is of paramount importance, since the induced electromagnetic gradients are highly sensitive to directionality [1]. As such, arrays of coils (**Fig. 2.D, E** and **F**) may be used to steer magnetic fields in any direction by independently controlling the pulse parameters and geometries of each component coil [19].

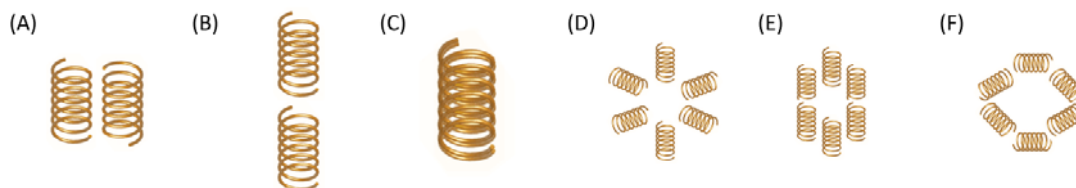


Fig. 2: μ MS coil configurations to increase strength, uniformity, focality or to steer the direction of the magnetic field: (A) figure eight (focality), (B) Helmholtz (uniformity), (C) bifilar (strength), (D) radial rotational field (steering), (E) axial rotational field (steering), and (F) circular loop (steering).

One of the greatest challenges to long-term implantation of μ MS is to minimize power consumption to make it comparable to that of ES. If the power requirements of μ MS can be thus reduced, the technology can be miniaturized to create fully implantable systems and the technology be easily adapted to a number of chronic therapeutic applications. In this manuscript we show that it is possible to lower the μ MS power consumption by increasing the gradient of the induced current density by: (a) utilizing coils with high-permeability core materials, (b) optimizing the shape of the

stimulation waveform, (c) utilizing energy-harvesting circuit designs, (d) designing coils with low Q , and (e) designing optimized μ MS coil arrays.

This manuscript is divided into a theoretical section that considers the power calculations and presents an expression for pulse design, a results section that outlines the Finite Element Method and presents tissue current-density distributions for surface mount inductors of 400, 200 and 100 μm diameter to investigate how these fields change at different frequencies of interest (i.e., from 100 kHz to 1 MHz) and with different magnetic permeabilities (i.e., from 1 to 10^6).

2. Theory

Neurons can be stimulated by passing a short pulse of current through a coil. This generates a time-varying magnetic field \mathbf{B} inside of and in the space surrounding each coil. In brain tissue, the time-varying magnetic field \mathbf{B} in turn generates an orthogonal electric field \mathbf{E} capable of evoking action potentials, according to Faraday's law. Neuronal compartments, such as axons parallel to the direction of the current density \mathbf{J} , are depolarized or hyperpolarized depending on the direction and strength of \mathbf{J} , but compartments orthogonal to \mathbf{J} are not affected. Thus, μ MS is capable of activating or inhibiting neurons in an orientation-specific manner using the energy stored in the magnetic field. An inductor is an ideal magnetic field generator, and it stores the magnetic field energy W generated by the supplied electric current i . The

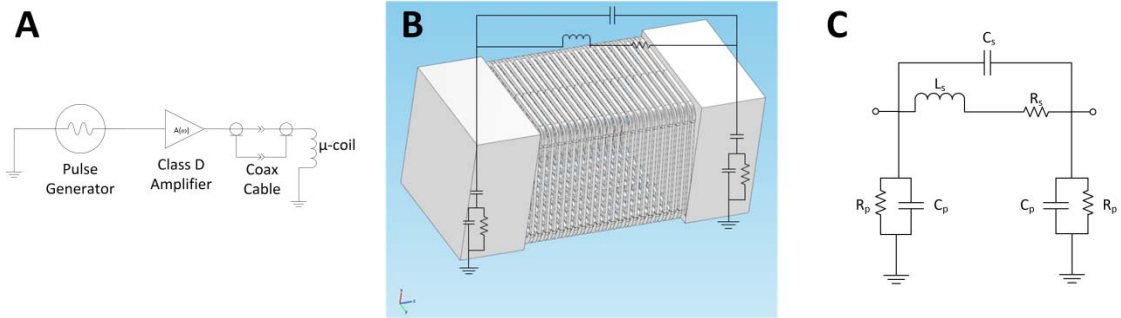


Fig. 3: In our investigations, the coil was driven by a class D amplifier (A). An N -turn μ MS coil (B) was studied using an equivalent electrical circuit (C), which takes into account different sources of losses. Magnetic flux losses that do not contribute to Joule heating constitute those contributing to microscopic magnetic stimulation of excitable tissue, thus μ MS optimization requires a proper low Q -factor design (e.g., spiral coils, see APPENDIX).

maximum energy that can be stored in the magnetic field of an ideal inductor is:

$$W = \frac{1}{2} \iiint \mathbf{J}(x, y, z) \cdot \mathbf{A}(x, y, z) dx dy dz = \frac{1}{2} Li^2 \quad (1)$$

where \mathbf{A} is the magnetic potential, and the curl is the magnetic flux density (i.e., $\mathbf{B} = \nabla \times \mathbf{A}$). In an actual inductor, the portion of the energy W that is lost is available for

eliciting neuronal activity, even though this loss reduces the Q-factor or the efficiency and the inductance of the coil.

The complex power (VA) in the N-turn square loop coil can be written as:

$$P_c = \frac{1}{2} \int_{-\infty}^{+\infty} |I(\omega)|^2 Z_c(\omega) d\omega \quad (2)$$

The power dissipated by the coil when driven by a train of pulses is:

$$P_d = N_s \int_{\beta} |I(\omega)|^2 \text{Re}(Z_c(\omega)) d\omega \quad (3)$$

Where N_s is the number of pulses per second, $Z_c(\omega)$ is the complex impedance of the coil and β is the frequency band of the pulse response.

The general form of the Ampere's equation which includes the displacement currents and is based on the assumption of time-harmonic fields is:

$$\nabla \times \mathbf{H} = (j\omega\epsilon_0\epsilon_r + \sigma) \mathbf{E} + \mathbf{J}^e \quad (4)$$

where \mathbf{J}^e is the current that flows through the μ MS coils, and σ is the conductivity of the coil-wire metal or the tissue. The *constitutive relations* of the material and the definition of the magnetic potential \mathbf{A} are:

$$\mathbf{H} = \frac{\mathbf{B}}{\mu_0\mu_r} \quad (5)$$

$$\mathbf{B} = \nabla \times \mathbf{A} \quad (6)$$

The electric field in the tissue is expressed by Faraday's law:

$$\mathbf{E}_t = -j\omega\mathbf{A} - \nabla\phi \quad (7)$$

where ϕ is the scalar potential. In a manner similar to [20], it is assumed that $\nabla\phi = \mathbf{0}$ because ϕ is due solely to free charges and no such sources are present in the medium.

Combining eqs. (4-7), we obtain the time-harmonic equation of the Maxwell-Ampère's law:

$$(j\omega\sigma - \omega^2\varepsilon_0\varepsilon_r)\mathbf{A} + \nabla \times \left(\frac{1}{\mu_0\mu_r} \nabla \times \mathbf{A} \right) = \mathbf{J}^e \quad (8)$$

Let us now consider the following cylindrical coordinates (r, φ, z) , where the axis of the coil is perpendicular to the z -axis and each turn of the coil can be approximated by a circle with radius r and potential V_r . The external current density has norm:

$$\mathbf{J}^e = \frac{\sigma V_r}{2\pi r} \mathbf{u}_\varphi \quad (9)$$

The induced currents were found by solving numerically (see *Results*) the following quasistatic approximation of Maxwell equations in cylindrical coordinates:

$$(j\omega\sigma - \omega^2\varepsilon_0\varepsilon_r)A_\varphi + \nabla \times \left(\frac{1}{\mu_0\mu_r} \nabla \times A_\varphi \right) = \frac{\sigma V_r}{2\pi r} \mathbf{u}_\varphi \quad (10)$$

where $\varphi \in [0; 2\pi]$ and \mathbf{u}_φ is the unit vector in the φ -direction inside the coil.

3. Pulse Design.

In order to understand which pulse shape minimizes the power consumption we study the equivalent-circuit of the μ MS coil (**Fig. 3, right**) as a lumped circuit [21]. The μ MS coil is modeled as a series resistance (R_s) and inductance (L_s). R_s is generated by the eddy current effect when the spiral trace is subjected to time-varying magnetic fields and is governed by Faraday's law [22]. Eddy currents are relevant only if the conductor thickness is greater than the skin depth:

$$\delta = \sqrt{\frac{1}{\pi\sigma\mu f}} \quad (11)$$

where σ is the conductivity of the traces (S/m), μ the permeability (H/m) and f the frequency (Hz). The bridge between the center of the spiral and one of the terminals generates direct capacitive coupling between the two terminals of the inductor, and is modeled by a feedthrough capacitance (C_s). The capacitance (usually an oxide) between the spiral and the substrate is denoted as the capacitance (C_p). The capacitance and resistance of the silicon substrate are modeled as a parallel operator (i.e., $//$ or $Z_1//Z_2 = (Z_1 \cdot Z_2)/(Z_1+Z_2)$) of a resistance (R_p) and capacitance (C_p) [23]. This equivalent circuit can be used to evaluate the complex power (VA) in the spiral coil, written in the frequency domain as a function of the impedance $Z_c(\omega)$ of the coil as

shown in **Fig. 3**. The frequency response of the coil equivalent circuit can be expressed by the following current term:

$$\begin{aligned}
I(\omega) &= \frac{V(\omega)}{Z_c(\omega)} = \frac{V(\omega)}{\left(\frac{1}{j\omega C_p} // R_p\right) // \left(\left(\frac{1}{j\omega C_s} // (j\omega L_s + R_s)\right) + \left(\frac{1}{j\omega C_p} // R_p\right)\right)} = \\
&= \frac{V(\omega) \left(\begin{array}{c} R_p + R_s + R_p^2 R_s + j\omega (L_s + R_p^2 C_p + 2R_p R_s C_p + R_p R_s C_s) - \\ \omega^2 (2R_p C_p L_s + R_p C_s L_s + R_p^2 R_s C_p^2 + R_p^2 R_s C_p C_s) - \\ j\omega^3 (R_p^2 C_p^2 L_s + R_p^2 C_p C_s L_s) \end{array} \right)}{\left(1 + R_p R_s + \omega j (R_p C_p + R_p L_s + R_s C_s) - \omega^2 C_s L_s - \omega^2 R_p R_s C_p C_s - j\omega^3 R_p C_p C_s L_s\right) (1 - j\omega R_p C_p)} \\
&\approx \frac{j\omega C_s (R_s + j\omega L_s)}{R_s + j\omega (C_s + L_s)} V(\omega)
\end{aligned} \tag{12}$$

With the approximation assumption is that parallel stray impedances due to packaging are negligible or that $R_p \ll R_s$ and $C_p \ll C_s$. The ideal pulse is one that provides a maximal electric field in the tissue with which to excite neurons while minimizing the energy, thus improving microcoil battery life in the context of long-term implantation. The electromotive force within the tissue is proportional to the first time-derivative of the current flowing through the coil, or in frequency space:

$$\mathbf{E}_t = -j\omega \mathbf{A} \propto -j\omega I(\omega) \tag{13}$$

The ideal current stimulation is a pulse $I(\omega)$ which minimizes the total complex power and maximizes $di(t)/dt$, or in frequency domain:

$$\begin{aligned}
&\int_{-\omega_0}^{+\omega_0} I(\omega)^2 Z_c(\omega) d\omega - j\omega I(\omega) \Big|_{-\omega_0}^{+\omega_0} = \int_{-\omega_0}^{+\omega_0} \left[I(\omega)^2 Z_c(\omega) - j \frac{d[I(\omega)]}{d\omega} \right] d\omega = \\
&\int_{-\omega_0}^{+\omega_0} [I(\omega)^2 Z_c(\omega) - j\omega I'(\omega) - j I(\omega)] d\omega = \int_{-\omega_0}^{+\omega_0} [I(\omega)^2 Z_c(\omega) - \\
&j\omega I'(\omega)] d\omega - \\
&jI_0
\end{aligned} \tag{14}$$

where $I_0 \in \mathfrak{R}$ is the mean of the Hermitian solution $I(\omega)$, and the integral functional is minimized by means of calculus of variations [24]:

$$\tilde{\mathbf{H}}(I(\omega)) = \int_{-\omega_0}^{+\omega_0} [I(\omega)^2 Z_c(\omega) - \lambda j\omega I'(\omega)] d\omega \tag{15}$$

where ω_0 is the angular frequency of the limits of the symmetrical frequency band and λ is the Lagrangian multiplier.

c.1. Case: $Z_c(\omega) = j\omega L_s$

If we consider the simplified case of an ideal inductor, eq.(15) has a minimum/maximum only if the following Euler-Lagrange differential equation is satisfied:

$$1 + 2\omega L_s I(\omega) = 0 \quad (16)$$

which has the following solution:

$$I(\omega) = -\frac{1}{2\omega L_s} \quad (17)$$

or in time is a rectangular pulse:

$$i(t) = C u(\alpha t) \quad (18)$$

where $u(t)$ is the rectangular pulse. Both α and C are set experimentally by the neuronal firing threshold level and by the slew rate of the amplifier. Since the inductors are RF type $\alpha \approx 1 \text{ GHz}$ range, such a short pulse can be implemented in a real world stimulator as a very steep triangle function, which in turns produces (i.e., the time derivative) a rectangular pulse in the tissue.

In realistic pulses, a net neuronal activation or inhibition can often be achieved with μMS by driving the coil with a sharp rising edge followed by a slowly falling dip (or vice versa), so that the resulting pulse is asymmetric producing an induced current pulse in the tissue above threshold in the raising edge followed by a sub-threshold current in the falling edge (or vice versa) (**Fig. 4**, top). The sub-threshold rectangular pulse is needed to drive the coil back to resting state (i.e., zero current in the coil) to minimize power consumption and coil heating. Furthermore, this sub-threshold pulse maybe used for energy harvesting, since the second sub-threshold pulse drains the coil from the magnetic energy stored (**Fig. 4**, in red), which can be captured by an energy-harvesting capacitor (**Fig. 4**, bottom).

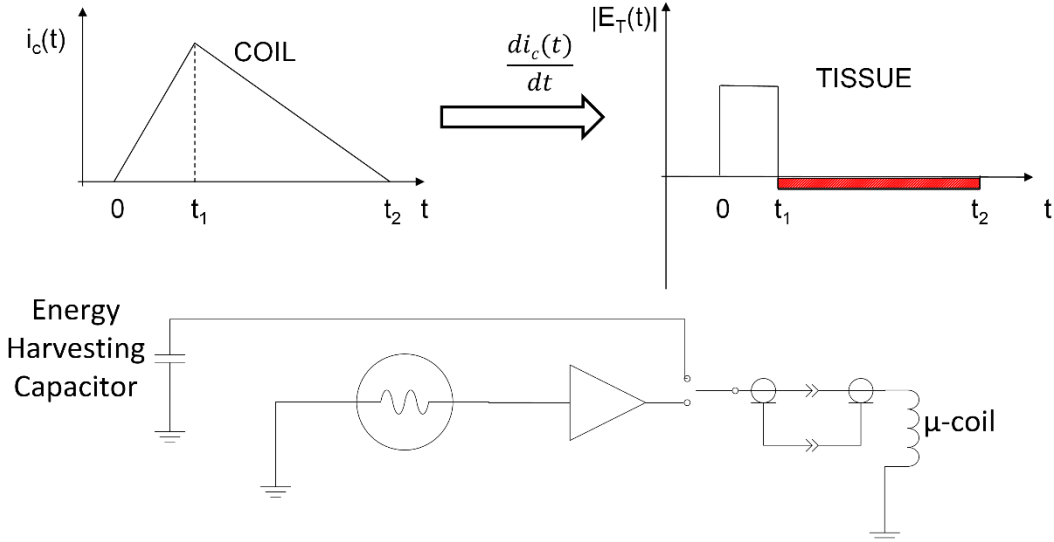


Fig. 4: (Top) An asymmetric triangular current pulse in the coil can be used to create two rectangular pulses in the electric field strength close to the μMS in the tissue, one above and one below threshold as commonly done in electrical stimulation for charge balancing. The second sub-threshold pulse drains the magnetic energy stored in the coil (in red), which can then be captured by an energy-harvesting capacitor. (Bottom) A switch capacitor design to capture the energy stored in the coil during the sub-threshold pulse.

c.2. Case: $Z_c(\omega) = j\omega L_s + R_s$

In this case, we have the Euler-Lagrange differential equation:

$$2(R_s + j\omega L_s)I(\omega) + j = 0 \quad (19)$$

with its solution:

$$I(\omega) = -\frac{1}{2} \frac{j R_s + L_s \omega}{R_s^2 + L_s^2 \omega^2} \quad (20)$$

or in time:

$$i(t) = C u(\alpha t) e^{-\beta t} \quad (21)$$

where $\beta = R_s/L_s$.

c.3. Case: $Z_c(\omega) = (j\omega L_s + R_s)//C_s$

In the RLC case, the Euler-Lagrange differential equation related to eq.(15) becomes:

$$1 - \frac{j\omega C_s (R_s + j\omega L_s)}{R_s + j\omega (C_s + L_s)} I(\omega) = 0 \quad (22)$$

with the solution:

$$I(\omega) = -\frac{1}{2\omega C_s} \frac{R_s - j\omega (C_s + L_s)}{\omega L_s - jR_s} \quad (23)$$

or the inverse Fourier Transform is:

$$i(t) = \begin{cases} C u(\alpha t) e^{-\gamma t} \left(\cos(\omega_d t) - \frac{\gamma}{\omega_d} \sin(\omega_d t) \right) & \omega_0 > \gamma \\ C u(\alpha t) e^{-\gamma t} (1 - \gamma t) & \omega_0 = \alpha \\ C u(\alpha t) e^{-\gamma t} \left(\cosh(\omega_d t) - \frac{\gamma}{\omega_d} \sinh(\omega_d t) \right) & \omega_0 < \alpha \end{cases} \quad (24)$$

4. Methods.

The Finite Element Method (FEM) is used here to characterize power dissipation, and induced currents in the μ MS coils. The simulations were performed in Multiphysics 4.3a (COMSOL, Burlington MA) FEM modeling using the AC/DC module [25]. The geometry consisted of a cylindrical container 3 mm in radius and 3mm in height, enclosing various objects: a physiological solution, a quartz core surrounded by a copper solenoid, and copper cylindrical terminals at the top and bottom. The FEM calculations were performed using a model consisting of a cylindrical inductor/coil with a 400- μ m radius (referred to as a “0402”) a height of 1 mm, a 200- μ m radius (a “0201”) a height of 0.5 mm, and a 200- μ m radius (a “01005”) a height of 250 μ m. The 0402, 0201 and 01005 coils respectively comprised 21, 15 and 10 turns (**Fig. 5**), and were positioned inside a uniform volume conductor representing the physiological solution or neuronal tissue with similar electrical characteristics.

The FEM method was used to solve eq.(10) numerically with respect to the magnetic potential \mathbf{A} in the frequency domain at different frequencies of interest (i.e., from 100 kHz to 1 MHz) and with different magnetic permeabilities (i.e., from 1 to 10^6). The subdomain settings are defined by the properties of the materials and the initial conditions for each model. The material considered had the following properties: (*copper*) $\sigma = 5.998 \cdot 10^7 S/m, \epsilon_r = 1, \mu_r = 1$, (*air*) $\sigma = 0 \frac{S}{m}, \epsilon_r = 1, \mu_r = 1$, and (*physiological solution*) $\sigma = 3 S/m, \epsilon_r = 30, \mu_r = 1$.

All the surface boundaries around the outer shell of the cylinder (**Fig. 5A**), to $n \times \mathbf{A} = 0$ (i.e., magnetic insulation). The initial conditions were all $\mathbf{A} = 0$ (i.e., null magnetic potential) throughout the entire geometry. The mesh was a Delaunay set with adaptive refine meshing option and a maximum element size of 220 μ m on all domains. The voltage in each turn was the same for all the simulations and was found experimentally to be approximately a value of $V_T = 4.19$ V.

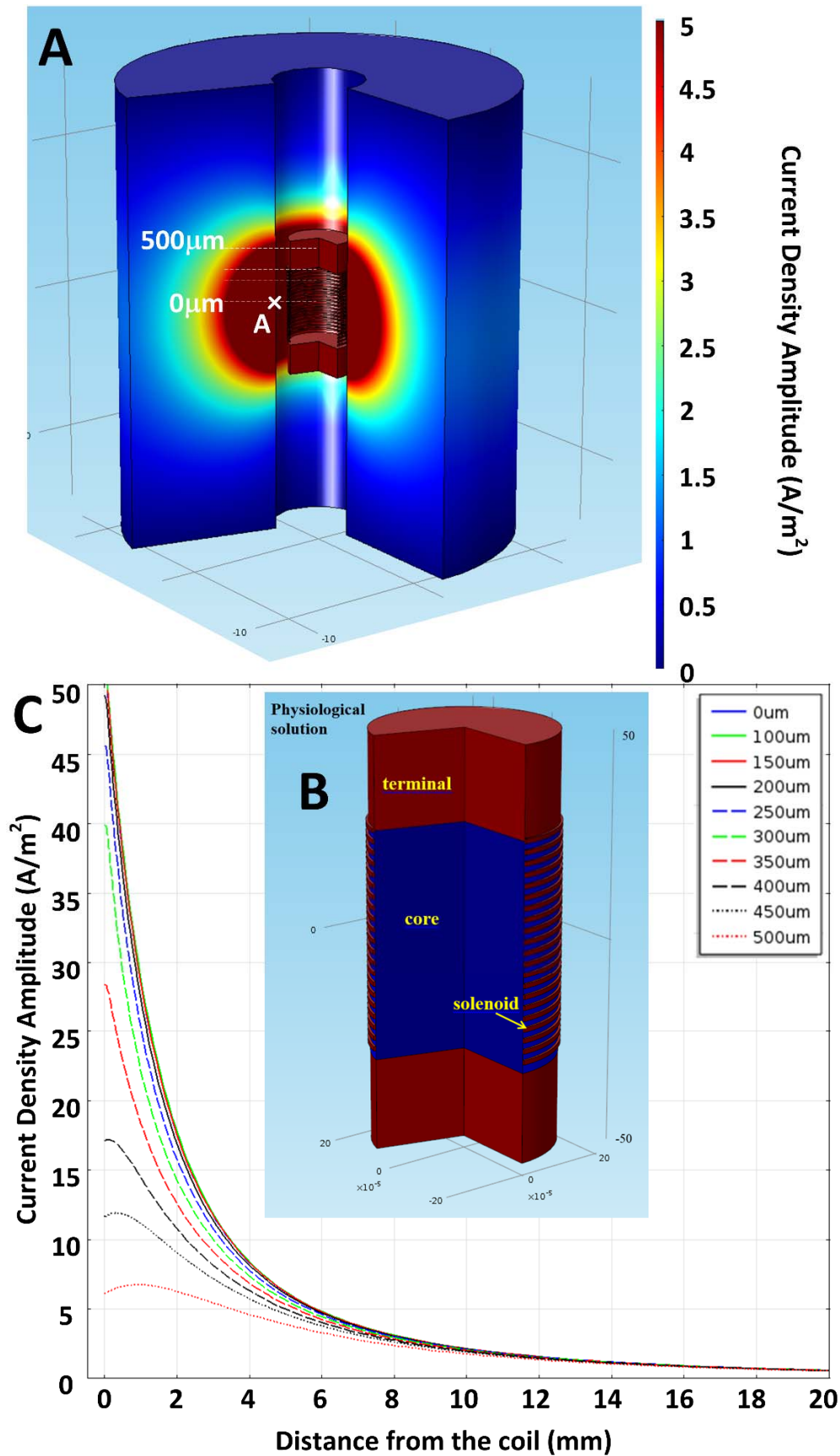


Fig. 5: (A) 3D Current density distributions, (B) geometry used in the FEM simulations and (C) current density along the x or y axis at distances shown in Fig. 5A from the center of a 400µm diameter coil.

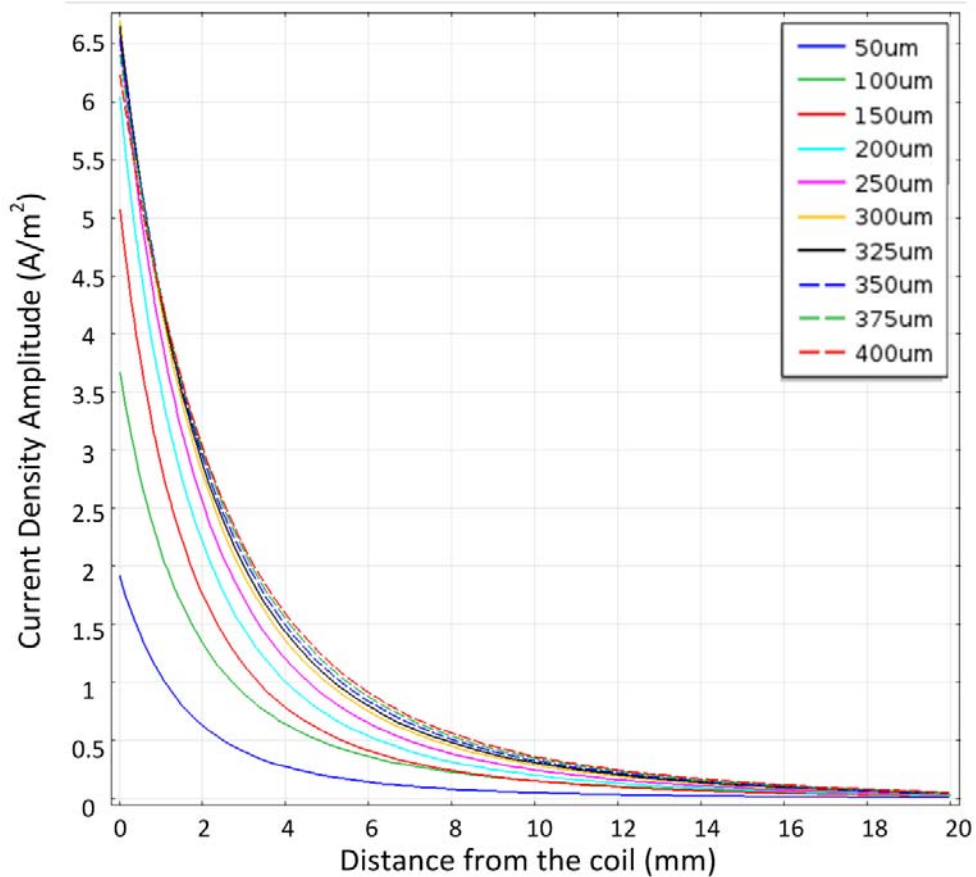
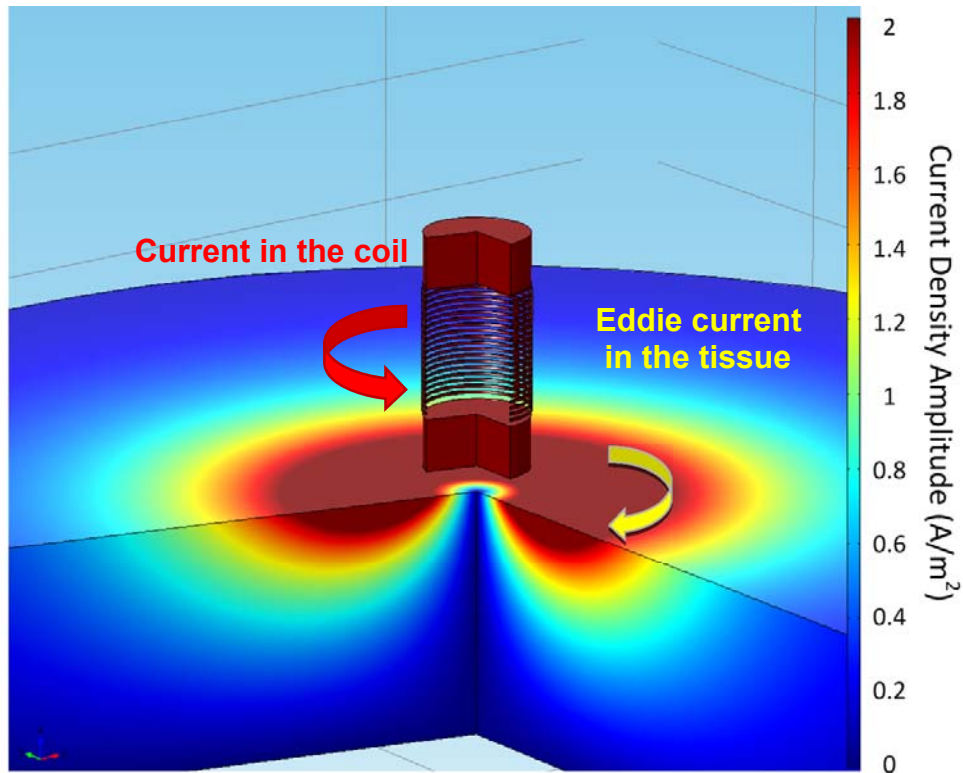


Fig. 6: (Top) 3D Current density distribution, showing Lenz's law for one of the two possible current directions. (Bottom) Current density distributions below the tip of the coil and along a parallel to the axis of the coil at different radial distances from the center of the 400µm diameter coil.

5. Results.

We first present data concerning the current density distribution inside and around coils of different sizes, in order to characterize how small the coil can be made while remaining capable of stimulating neurons.

The current induced by the coil follows a circular path (eddy current) in the tissue, such that current densities in the coil in the tissue have opposite directions (i.e., Lenz's law see **Fig. 6**, top). The distributions around (**Figs. 5, 7, and 9**) and below (**Figs. 6, 8, and 10**) the coil are presented. The current density distribution within the tissue is dependent on the diameter of the coil (**Figs. 5-10** top), with higher induced fields adjacent to the coils and fields with lower local maxima in close to the coil terminals. The radial distributions of the current densities at different heights (**Fig. 5** top) are all nonlinear, regardless of coil size (**Figs. 5-10**, bottom). With regard to current density distribution around the coil (**Figs. 5, 7, and 9**), only the current densities radially along a line radiating out from the coil (i.e., $z=0-350\mu\text{m}$) are decreasing monotonically, while along the rest, the current density will approach maximum and then further decrease. Below the terminal (**Figs. 6, 8, and 10**), at a given radial distance all the current densities are monotonically decreasing along the radial lines, since the local maxima are located inside each terminal. Along the $400\mu\text{m}$ outer diameter (OD) of the coil, the current density norm peaks at 50 A/m^2 (**Fig. 5**, bottom) for currents at a distance of $100\mu\text{m}$ from point midway between the coil terminals and drops to 4.5 A/m^2 at $100\mu\text{m}$ from the outer edge of the terminals (**Fig. 6**, bottom). At the half height of the coil (i.e., $z=0$), the current density curve was fit with an exponential equation using the coefficients given at the top of **Table 1**. This produced an excellent fit, with an R-square/adjusted R-square of 0.9999 and a root-mean-square error (RMSE) of 0.172.

In the $200\mu\text{m}$ OD coils (**Fig. 7**, bottom) the geometry is scaled to half the diameter of the $400\mu\text{m}$ coil, hence the peak current density at $100\mu\text{m}$ from the midpoint between the coil terminals is halved, to 25 A/m^2 . However, at $100\mu\text{m}$ from the outer edge of the terminals the decrease is only 3 A/m^2 , 33% of that obtained with the $400\mu\text{m}$ coil (**Fig. 8**, bottom). The second row of **Table 1** presents the current density coefficients derived by fitting the data with an exponential function, with an R-square/adjusted R-square goodness-of-fit value of 0.9996 and RMSE of 0.2959.

<i>Diameter</i>	p_1 (95% conf bounds) A	p_2 (95% conf bounds) A/m	q_1 (95% conf bounds) m^{-1}	q_2 (95% conf bounds) m^{-2}
400 μm	14.47 (13.8, 15.14)	36.88 (36.26, 37.5)	-1888 (-1948, -1828)	-8045 (-8203, -7886)
200 μm	40.44 (39.49, 41.39)	9.256 (8.247, 10.27)	-1.353 (-1.392, -1.313) 10^4	-2824 (-3063, -2584)
100 μm	35.65 (35.03, 36.28)	8.953 (8.291, 9.614)	-2.62 (-2.674, -2.565) 10^4	-5577 (-5903, -5252)

Table 1: Coefficients of the exponential function: $J(r) = p_1 \cdot \exp(r \cdot q_1) + p_2 \cdot \exp(r \cdot q_2)$ or the distribution current densities perpendicular and at the midpoint of the coil axis

Similarly, with the 100 μm OD coils (**Fig. 9**, bottom), the geometry scales to half that of the 200 μm OD coils. Hence the peak current density at 100 μm from the midpoint between the coil terminals also decreased by 50% (12.5 A/m²), with a negligible change in current density at 100 μm from the terminals, where current peaks at 3 A/m² (**Fig. 10**, bottom). Thus peak densities at a distance of 100 μm from the coil at its midpoint (**Fig. 5**, point **A**) are proportional to the coil diameter. However, peak densities measured at 100 μm from the terminals do not vary proportionally with respect to coil diameter. Indeed, the 200 μm coil revealed a 33% decrease in current density with respect to the 400 μm coil, while the 200 and 100 μm diameter coils were virtually identical in this regard. The current density norm below each terminal exhibits a similar monotonic decrease with respect to coil size (**Fig. 6, 8**, and **10** bottom). Current density values at the midpoint were fitted with the expression given at the bottom of **Table 1** along with the coefficients so derived. Excellent fits were thus obtained (R-square/adjusted R-square: 0.9998 and the RMSE is 0.161).

The current density norm induced in the tissue increases linearly with the frequency of the sinusoidal current in the coil, following Faraday's law in the frequency domain ($\mathbf{J}_t = \sigma \mathbf{E} = -j\omega\sigma \mathbf{A}$). In the 400 μm OD coils (**Fig. 11**, top), at a distance of 300 μm from the coil windings, the current density norm doubles from 18 A/m² to 36 A/m² when the frequency increases from 100kHz to 200kHz. A proportional increase in current with frequency is observed at all frequencies for the 200 μm OD coils (**Fig. 11**, middle) and for the 100 μm OD coils (**Fig. 11**, bottom). The current density norm increases non-linearly, however, with respect to the magnetic permeability for all the coils tested (**Fig. 12**). Finally, the electric field spatial gradient increases linearly with coil diameter (**Fig. 13**).

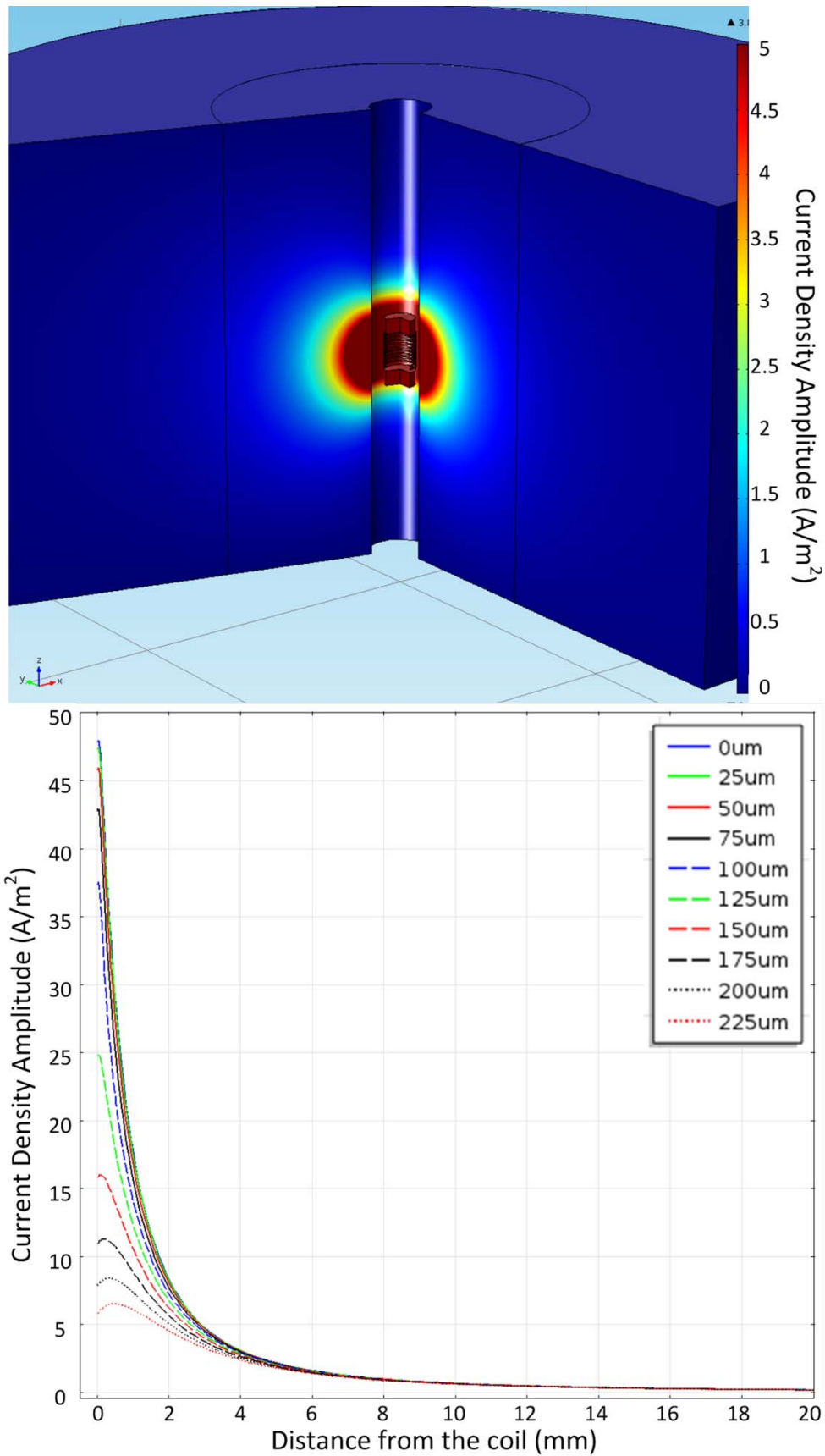


Fig. 7: (Top) 3D Current density distribution and (bottom) 1D current density distribution along the x or y axis at distances shown in Fig. 5A from the center of a 200µm diameter coil.

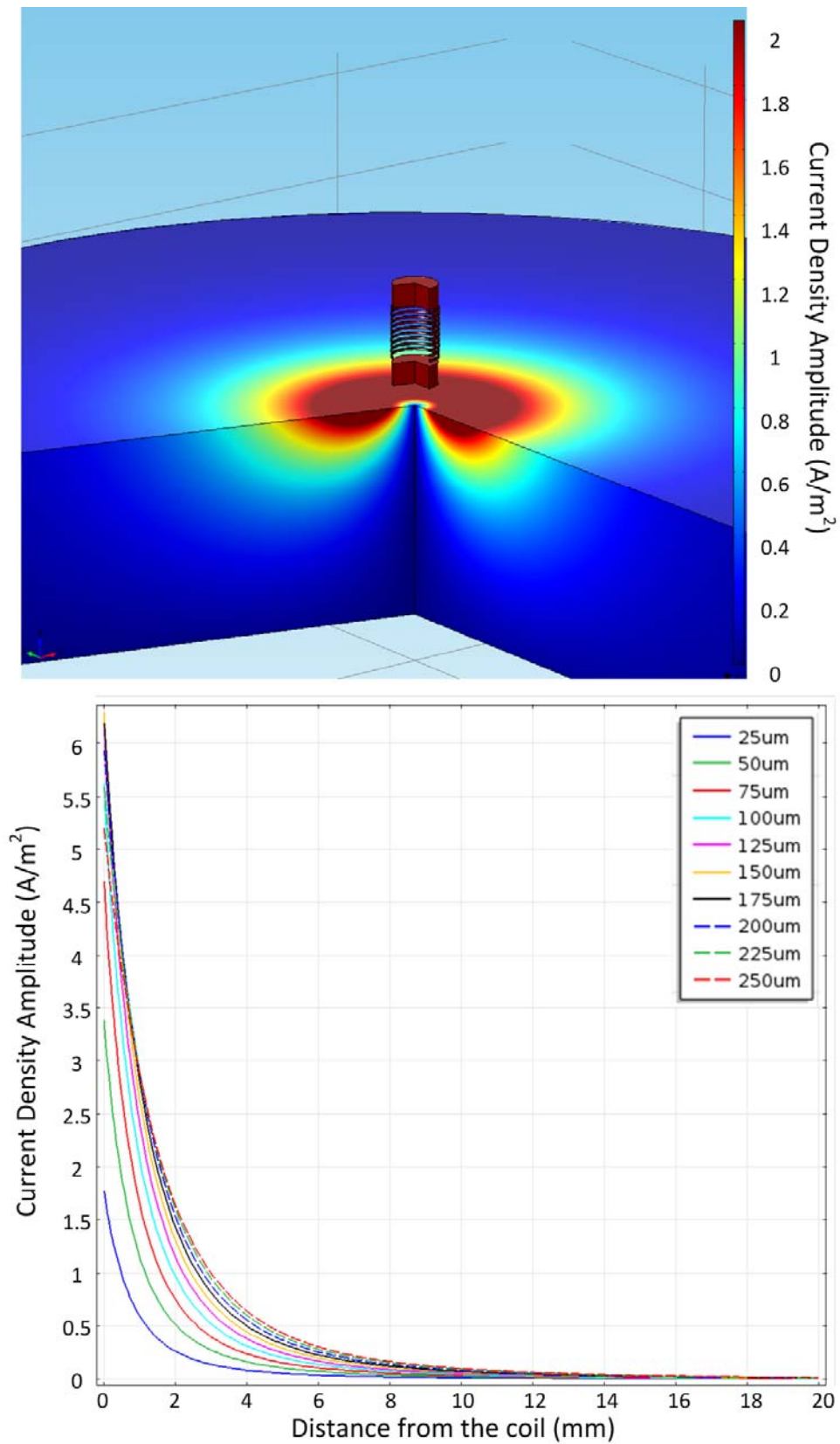


Fig. 8: (Top) 3D Current density distribution and (bottom) 1D current density distributions below the tip of the coil and along a parallel to the axis of the coil at different radial distance from the center of the $200\mu m$ diameter coil.

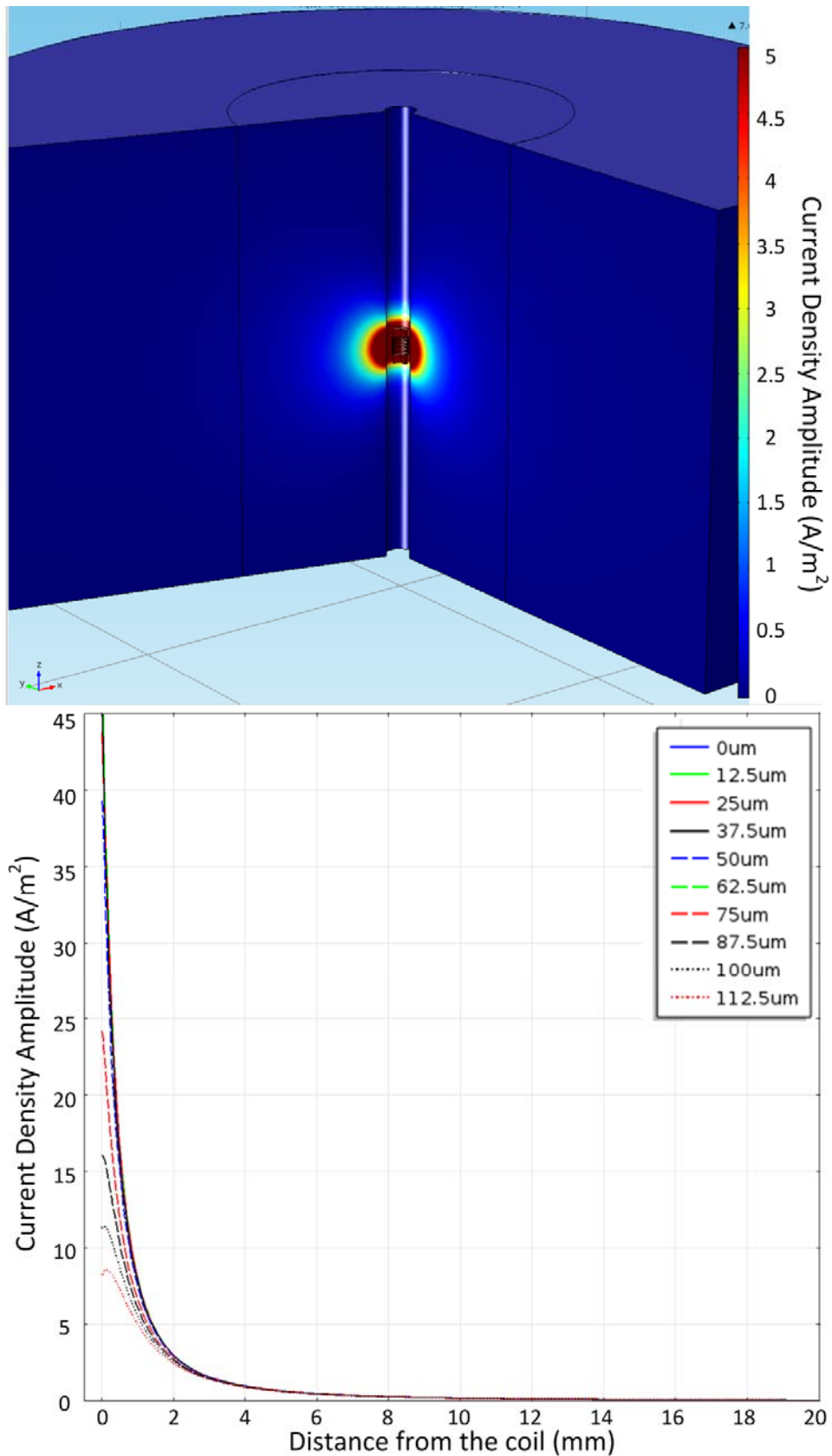


Fig. 9: (Top) 3D Current density distribution and (bottom) 1D current density distribution along the x or y axis at distances shown in Fig. 5A from the center of a 100µm diameter coil.

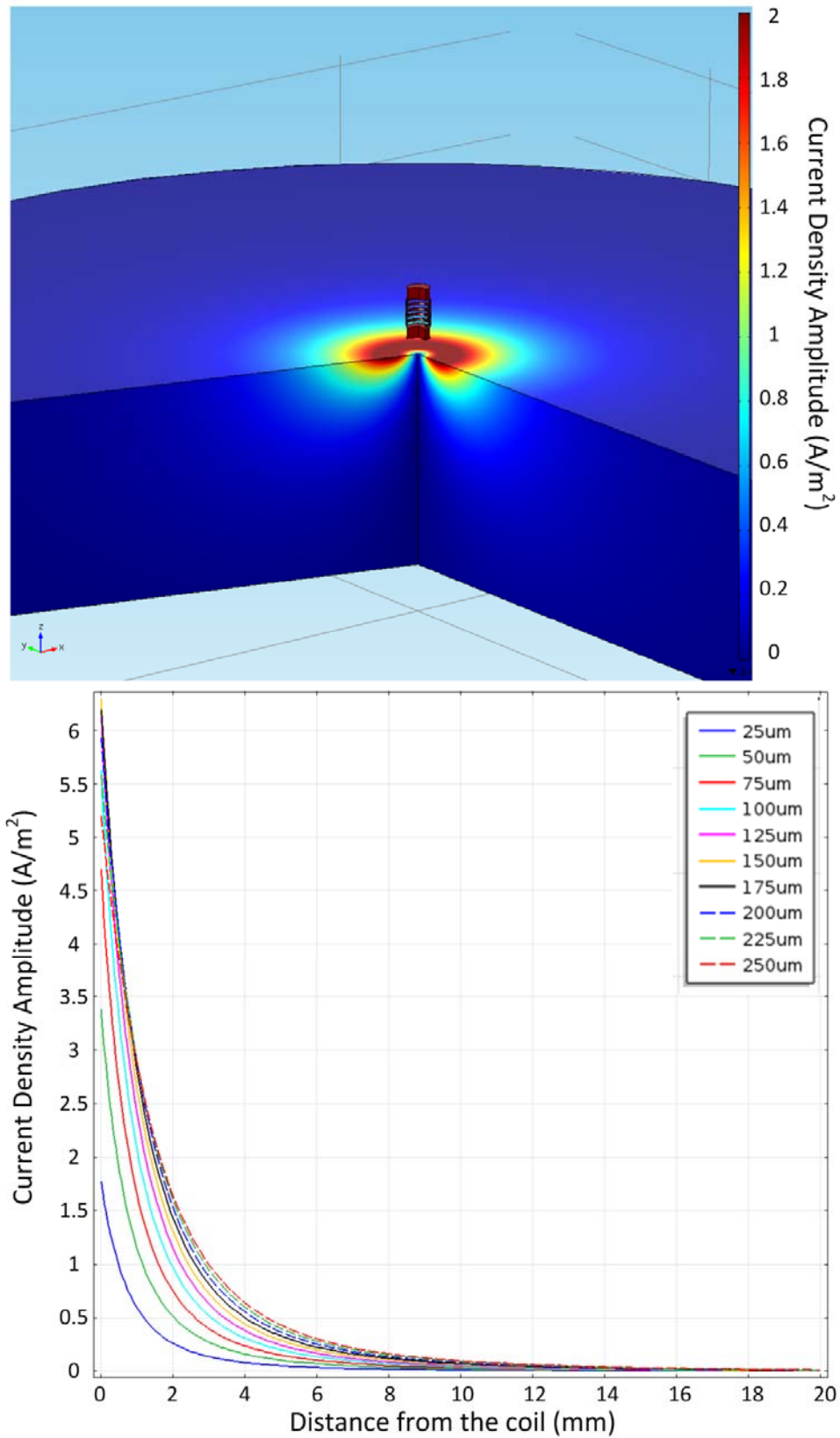


Fig. 10: (Top) 3D Current density distribution and (bottom) 1D current density distribution below the tip of the coil and along a parallel to the axis of the coil at different radial distances from the center of the 100 μ m diameter coil.

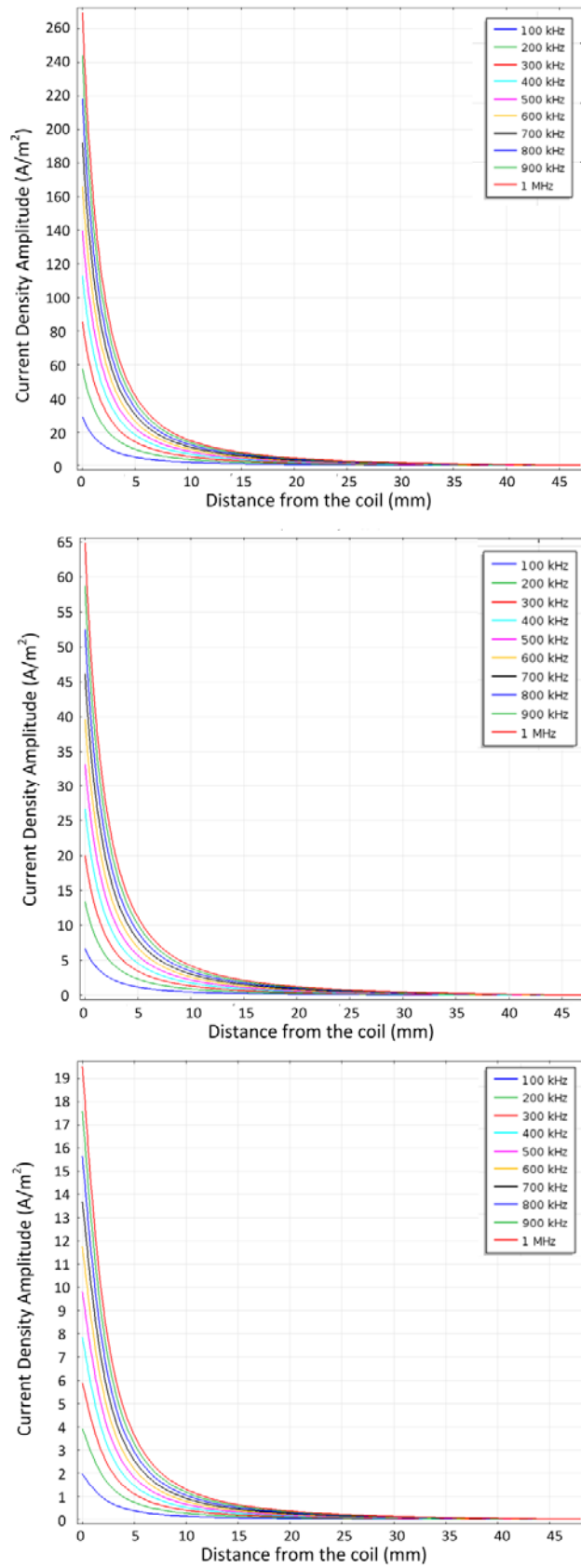


Fig. 11: Current density distributions along the z-axis with change in frequency for (top) 0402, (middle) 0201, and (Bottom) 01005 coils.

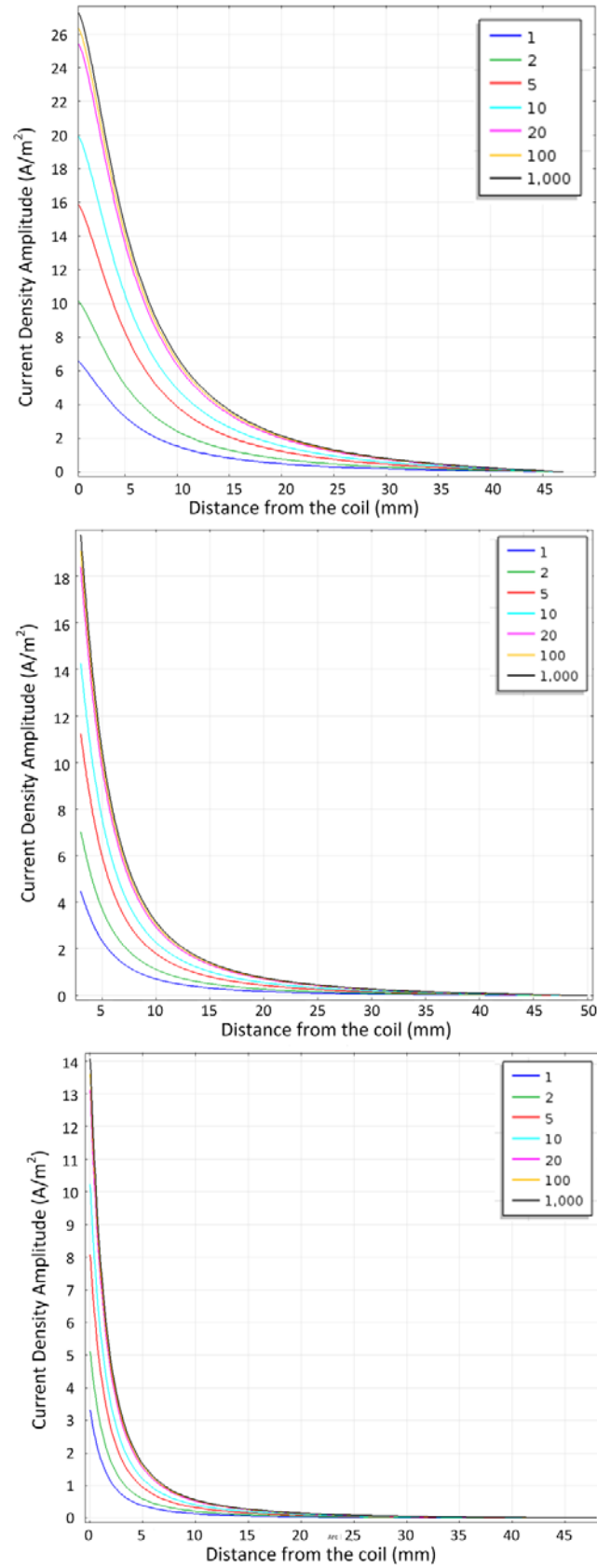


Fig. 12: Changes in horizontal current density distributions with respect to core relative magnetic permeability of (top) 400 μm , (middle) 200 μm , and (Bottom) 100 μm coils.

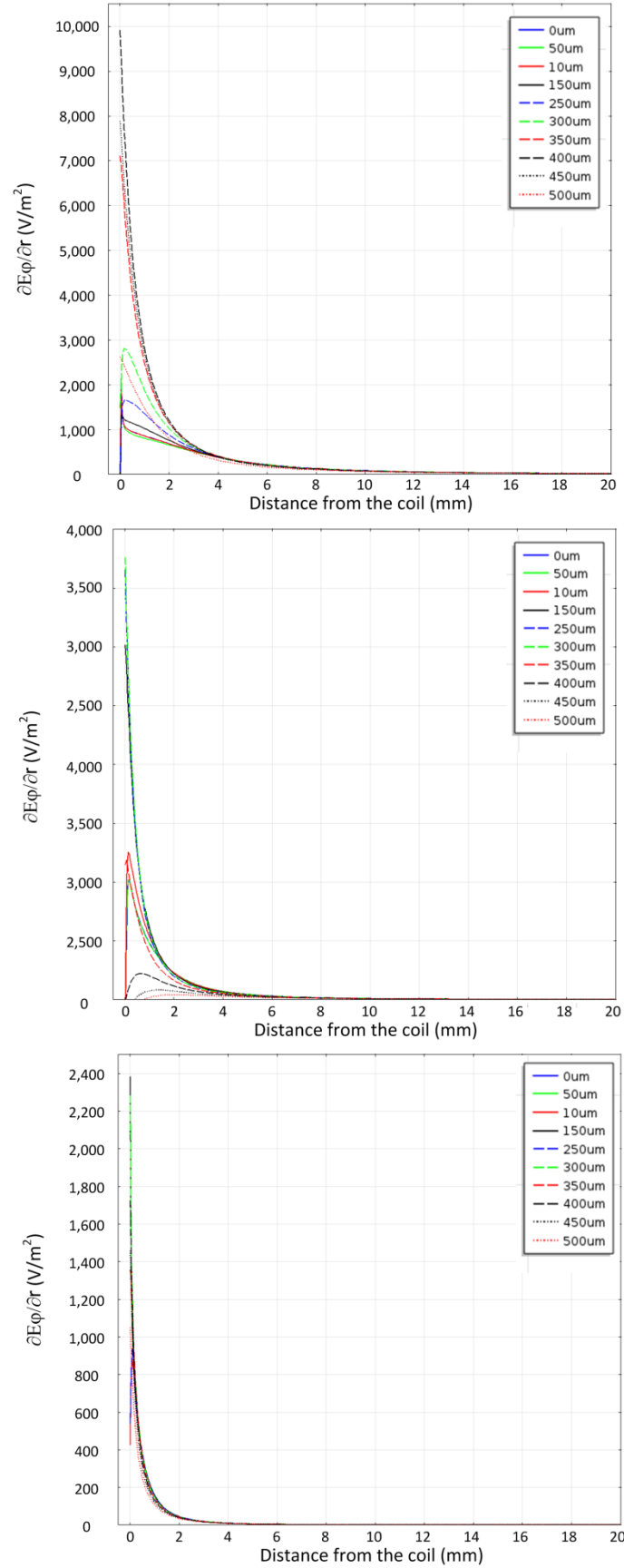


Fig. 13: Horizontal change in norm of the spatial gradient of the electric fields induced by (top) 400 μm , (middle) 200 μm , and (Bottom) 100 μm coils.

6. Discussion

Although neuronal stimulation using electrical techniques has proven quite useful for some applications, we have focused on μ MS because it offers several advantages over purely electrical methods. In order for an electrode to generate current, it needs to be in contact with a conductive media (e.g. excitable tissue). However, a coil can induce a current from a distance (e.g., through an insulating layer). However unlike TMS, these μ MS coils can be placed within or immediately adjacent to the neural tissue, greatly reducing the power needed to evoke neuronal activity. Here we have explored the effects of coil geometry, stimulation frequency and magnetic permeability on the resulting current density norm. Our results demonstrate that: (a) μ MS does not require charge-balanced stimulation waveforms as in electrical stimulation, (b) Microcoils of different sizes and core material permeabilities produce non-linear changes in the electric field induced in the tissue, and (c) the ideal shape for a stimulation pulse is one with maximum slope or slew rate, at least from an energy efficiency point of view, though *in vivo* experiments must yet confirm that such a pulse will indeed excite neural tissue.

The distance at which certain current-density norms peak has been observed to scale in approximate proportion to the diameter of the coil. For instance, the peak for a distance of $300\mu\text{m}$ from the $400\mu\text{m}$ OD coil (Which is the distance this μ MS coil activates retinal ganglion cells, albeit at a slightly lower, 70kHz , frequency [1]) is 18 A/m^2 . For a $200\mu\text{m}$ OD coil, the same peak current density norm appears at approximately $150\mu\text{m}$, and for the $100\mu\text{m}$ coil, the peak occurs at $75\mu\text{m}$ OD.

In electrical stimulation, using a bipolar electrode pair, the 'cathode' or source, injects a current that depolarizes the neuronal membrane, driving the potential towards a more positive E that can generate an action potential. At the 'anode' or sink, the axonal membrane potential is hyperpolarized towards a more negative potential that can inhibit the propagation of an action potential. The principal issue in the design of electrical stimulation pulses is that charges may accumulate over time, producing electrolysis byproducts that can damage or produce inflammation of neural tissue. In contrast, neither sinks nor sources exist when a current is induced by a magnetic field. This current consists of a rotating field that mirrors the current flow in the coil. The property of having no net sources or sinks as derived from the Maxwell Equations insures that, with μ MS, there is never a net charge buildup.

Microelectrodes deliver currents into the surrounding tissue by means of resistive coupling at the point of tissue-electrode contact. Our alternative approach is to generate currents by means of inductive, rather than resistive, coupling. As demonstrated by traditional macroscopic TMS, we know that magnetically-induced currents can induce neural activity [26] and that its therapeutic use in treating neurological disorders has been studied for more than two decades [26, 27]. However, employing TMS in standard medical therapy is hindered by several technical and practical limitations, such as large device sizes, low spatial control and potential patient discomfort. TMS requires the coils to be relatively distant from the neural tissue, as opposed to μ MS, where coils can be placed in close proximity to the target tissue. The large distances involved in using TMS therapeutically has three major implications. First, TMS requires an extremely high current to drive the coils sufficiently to elicit neural activity. The current-driving sources utilized in TMS are many orders of magnitude higher than those of μ MS, and thus have significantly higher power requirements. Second, TMS generates strong magnetic

fields that stimulate broad cortical areas; offering limited spatial control over the elicited activity. In contrast, μ MS coils can be placed in close proximity to the neural elements, which allows more precise spatial control. While TMS is non-invasive, TMS can be uncomfortable for the patient because the induced current often activates the muscle overlying the skull, which is not with a factor in the use of μ MS (although μ MS is an invasive technology).

Theoretical studies of TMS include characterizing the electrical fields produced in neural tissue by magnetic stimulation [20] using coils in the centimeter-diameter range (i.e., 2, 3.5 and 5 cm). The results of such TMS simulation has shown only a limited ability to confine the induced current to a small brain area, and that such limitations could be at least partially overcome by more effective coil positioning and/or assembly. Other theoretical TMS studies make use of Eaton's model [28], comparing the effects of a 6-cm coil vs. two 5-cm coils arranged in a figure-eight geometry. The latter generated a more symmetrical, focal, and deeper E-field distribution than did the single coil. Eaton's model showed that a current of 3,700 A with a 200- μ s rise time, running through a single winding, would induce a 18.75 V/m peak E-field, which is the theoretical threshold [29] for exciting a 10- μ m nerve fiber. To achieve the same degree of stimulation, the figure-eight coil needs a 30% lower peak current, and the area of cortex thus stimulated is more focused. Thus, the results of Eaton's model (albeit scaled down in the case of the μ MS coils) raises the expectation that the figure-eight geometry will allow us to reach deeper into the tissue, while achieving more focal stimulation than with TMS.

The use of a magnetic field to generate current flow in tissue is extremely inefficient from an energy standpoint with respect to its capacity for inducing electrical fields or currents in a medium. Surprisingly, our hypothesis is that the opposite may prove true for neural stimulation at the microscopic level. One important difference between electric and magnetic field is that the magnitude of the latter is well known to fall off much more rapidly with distance (e.g., cubic vs. quadratic laws for electric vs. magnetic dipoles in empty space). Our hypothesis is based on the prediction by various activation models [14] that the field gradient, rather than its strength, is primarily responsible for neural stimulation. The FEM simulations confirm that a very high (i.e., 83 V/m²) electric field gradient in the physiological solution at the distances of interest, between 50 μ m and 125 μ m from the μ MS coil. On the other hand, the gradient is much smaller than the one used, for example, in our simulations involving relatively large (i.e., 6mm) electrodes [30].

Recently it has been demonstrated that μ MS is capable of eliciting neuronal activation, both *in vitro* [1] and *in vivo* in inferior colliculus neurons [2]. The *in vitro* experiments, performed in a retinal cell preparation, demonstrated that action potentials could be elicited by μ MS. It was also shown that neuronal activation was amplitude-dependent, whereby higher stimulation amplitudes resulted in more intense activation, and that varying the orientation of the coils relative to the neural substrate resulted in different activation patterns. Perpendicular orientations of the coil resulted in minimal activation, whereas parallel orientations resulted in maximal activation. In the *in vivo* experiments, it was demonstrated that μ MS of the dorsal cochlear nucleus resulted in neuronal activity in the inferior colliculus. Hence, μ MS can elicit neuronal activation within an interconnected neural circuit and is not restricted to modulation of local circuitry only. Yet despite these results, a number of key issues need yet to be addressed before μ MS can become useful in

fundamental research (e.g. as in Ekstrom et al. [31]) or in translational chronic neuromodulation therapies.

One primary issue relates to the amount of energy needed to sustain neuromodulatory effects using μ MS. The energy required for μ MS stimulation can be considerably reduced by employing at least these three strategies: (1) optimizing the stimulatory pulse shape, (2) designing coils with high permeability, and (3) recovering unused energy. First, energy could be optimized by using a more efficient pulse sequence. Traditional electrical stimulation pulse shapes are inadequate for μ MS stimulation since most of the energy is lost due to Faraday induction (eq. 7 and **Fig. 6**). Therefore, shorter pulses are preferable since less energy will be dissipated and larger current densities can be induced in the tissue. However, there are limitations in the duration of the excitation pulse since simulations suggest that with sinusoidal stimuli, the activation threshold increases monotonically with frequency when the stimulation plateau of a few kHz [32] is exceeded. In so optimizing stimulation sequences, one should endeavor to minimize the power and maximize the slope while still retaining the ability to activate neural tissue. Second, micro coils could be specifically designed for this application. For example, the long solenoid design used here optimizes the Q-factor but renders the bulk of the magnetic energy inaccessible. An alternative is the use of multiple, slimmer coils (i.e., spiral, see **APPENDIX**) or by using the principle of field summation. The dimensions of the coil can further be reduced using advanced MEMS construction techniques and by generating fields with even higher gradients. However, there are limitations on the magnitude of the magnetic field flux density obtainable by increasing size because of the aforementioned limits on current densities for various metals. Finally, inductors store energy (eq. 1) in the magnetic flux density, and it is well-known that this energy can be recovered. For example, the energy can be extracted from the magnetic flux density of the inductor by disconnecting the generator and connecting the coils to a capacitor. Therefore, it may be possible to recover unused energy in an implanted μ MS system and thus extend battery life. The ability to recover energy with a μ MS-based inductor is not possible with conventional stimulation employing a microelectrode, such as with DBS, where much of the power is dissipated as thermal energy.

There are two types of inductor core coils that are available in small, surface-mount packaging (i.e., 0402, 0201 and 01005, as used in the FEM simulations presented here): air and ferromagnetic. Ferromagnetic core coils may increase the inductance by three orders of magnitude, due to its higher permeability. However, the magnetic properties of the ferromagnetic cores induce losses and nonlinearities due to hysteresis that increase with slew rate or frequency and generate MRI artifacts. We chose the air coils for our *in vitro* [1] and *in vivo* [2] experiments because they are usually non-magnetic. Our inductors were tested and found to produce no T1 or T2* artifacts in the MRI [33]. Furthermore, air core inductors are designed for high-frequency currents with no significant distortion. The surface-mount, high inductance air coils are RF-MEMS-based technology and have only recently been introduced into the market [34]. The dimensions of the coils were: 1,000(L) \times 500(W) \times 350(H) μ m, 500(L) \times 250(W) \times 175(H) μ m and 250(L) \times 125(W) \times 85.5(H) μ m [35]. In theory, coil inductances can be estimated directly from their geometries using published formulas ([36] and **Appendix**). Each inductor tested had an inductance and DC resistance consistent with the data sheet ($\pm 10\%$), and the 4- Ω resistance was optimal for driving the 1-kW audio amplifier. The RF-field may produce local peaks of electric field and specific absorption rate

(SAR) because of the high conductivity of metals [5, 37, 38]. Since the SAR peak occurs in the tissue/metallic electrode interface [5], using electrical insulation may provide some protection against excessive heating. However, inductive heating may still be a possibility, even in the presence of an insulator and with large conductors (e.g., the terminals in the coil model in **Fig. 3B**).

7. Conclusion

We have investigated micromagnetic stimulation (μ MS) because it has several advantages over electrical stimulation methods. For example, μ MS does not create sinks or sources when a current is induced by a magnetic field, and thus it does not suffer from the charge buildup that may occur with electrical stimulation. The simulation data indicate that the current densities do not scale linearly with the coil size, but reduce approximately quadratically as coil diameter is reduced. Thus, microscopic magnetic neuronal stimulation with coils approximating the size of the cell or smaller maybe feasible if positioned very close to or even inside the cell. Furthermore, energy efficiency can be achieved by utilizing the recommended pulse, constructing microcoils with high-permeability cores (albeit losing MRI compatibility) and by harvesting energy from the coil immediately after stimulation. Energy efficient μ MS may allow for direct deployment in the clinical field on patients, who will benefit from the reduced immunological response, MRI safety and enhanced control offered by μ MS over traditional electrical stimulation.

8. APPENDIX

INDUCTANCE CALCULATION FOR A RECOMMENDED COIL GEOMETRY

Inductance calculations for different types of inductors can be found in several seminal works [39-46]. Here we will consider planar spiral square coils (**Fig. 14**, top) since these types of coils have the potential to offer the best performance in μ MS coil applications, as the magnetic flux is readily accessible to the tissue (**Fig. 14**, bottom). For planar spiral square coils, it has been shown that the optimal Q-factor can be achieved when the D_e/D_i (i.e., the ratio between external and internal diameters) is 5 [47], thus this is not optimal for future μ MS coil designs, and a lower or higher value should be used depending on the degree of focus needed for the stimulation. The total inductance has been estimated [48, 49] as the sum of the self-inductance and the positive and negative mutual inductances:

$$L_s = L_0 + M_+ + M_- \quad (25)$$

where L_s is the total inductance. L_0 , is the sum of the self- inductances of all the straight segments, M_+ is the sum of all the positive mutual inductances or when the current flow in two parallel conductors is in the same direction and M_- for currents in the opposite direction. The current on opposite sides of conductors are parallel to one another, whereas the currents in adjacent segments are orthogonal. Given that μ -magnetic stimulation is typically low frequency where dispersion and loss mechanisms are not predominant, we can take advantage of symmetry and the fact that segments with orthogonal current have zero mutual inductance. The inductance

can be well approximated by the sum of the self-inductance of adjacent segments and the mutual inductance between opposite conductors [50]:

$$L_s = \mu_0 N^2 C_1 \frac{l+i}{4} \left[\log \left(C_2 \frac{l+i}{l-i} \right) + C_3 \frac{l+i}{l-i} + C_4 \left(\frac{l+i}{l-i} \right)^2 \right] \quad (26)$$

This simple approximation has an error lower than 8% for $s \leq 3w$, since smaller spacing improves the magnetic coupling between loops and reduces the total length of the spiral. Where (see also **Table 2**):

N : total number of segments in the spiral

l : total length of the spiral (m)

i : inside diameter of the spiral (m)

w : width of the traces (m)

t : thickness of the traces (m)

t_{sub} : thickness of the substrate (m)

s : spacing between segments (m)

s_u : spacing between traces and underpass (m)

T : number of turns

G_{sub} : conductance per unit area of the substrate (S/m²)

X_{sub} : capacitance per unit area of the substrate (S/m²)

ϵ_{sub} : dielectric constant of the substrate

ρ is the resistivity of the traces (Ω -m)

μ the permeability of the traces (H/m)

μ_0 the permeability of vacuum or $4\pi \cdot 10^{-7}$ (H/m)

f the frequency (Hz)

$k = 0.50049$

$C_1 = 1.27$

$C_2 = 2.07$

$C_3 = 0.18$

$C_4 = 0.13$

An online total inductance calculator using this and other approximations is available at:

<http://smirc.stanford.edu/spiralCalc.html>.

ALL THE PARAMETERS OF THE CIRCUIT IN **FIG. 2** CAN BE FOUND IN **TABLE 1 [23]**.

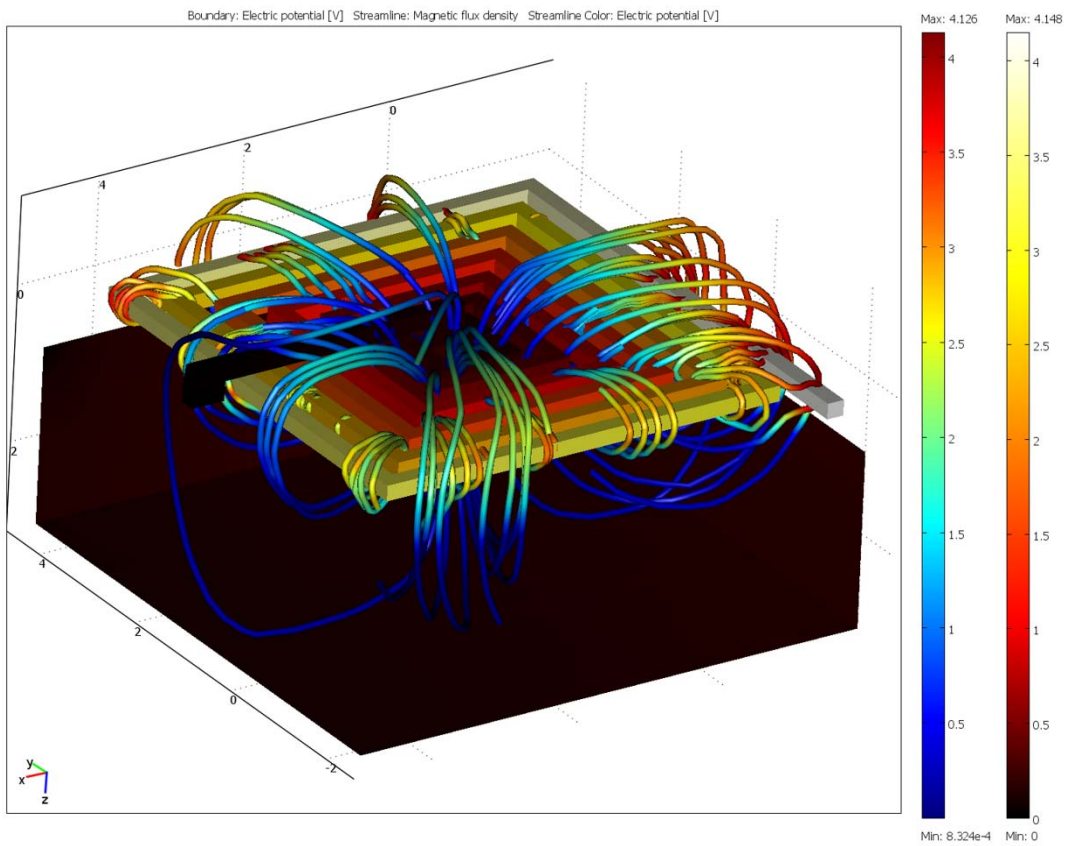
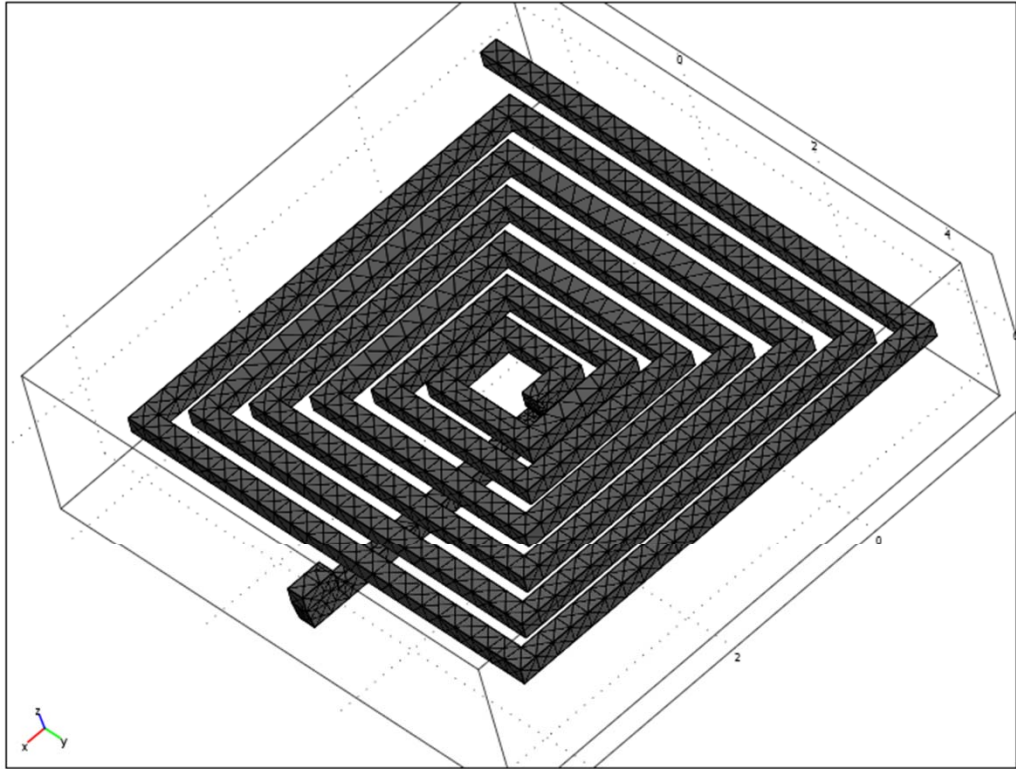


Fig. 14: (Top) The model of a seven-turn, square, spiral coil atop a slab of tissue undergoing FEM. (Bottom) Lines of magnetic flux and electric potential on the square spiral conductors. The magnetic flux enters the tissue and is not as confined to the core as with a solenoid coil.

9. Acknowledgements

Funding for this project was provided by the NEI (1R21EY020961-01), the NIBIB (1R21EB016449-01), the NCRR (P41-RR14075), and by the MIND Institute. We wish to thank S. Raiguel for his valuable comments on the manuscript. This work received support from Inter-University Attraction Pole 7/21, Odysseus G.0007.12, Programme Financing PFV/10/008, Geconcerteerde Onderzoeks Actie 10/19, FWO grants G090714N; G.0.622.08.N.10; G.0.831.11.N.10

<i>Parameters</i>	<i>Analytical Equation</i>
L_s	<i>eq.(4)</i>
R_s	$\frac{\rho l}{w t}$
C_s	$\frac{T w^2 \epsilon_{ox}}{s_u}$
C_{ox}	$\frac{w l \epsilon_{sub}}{2 t_{sub}}$
C_{sub}	$\frac{w l X_{sub}}{2}$
R_{sub}	$\frac{2}{l w G_{sub}}$

Table 2: Parameters used in inductance estimation.

10. References.

- [1] Bonmassar, G., Lee, S. W., Freeman, D. K., Polasek, M., Fried, S. I., and Gale, J. T., 2012, "Microscopic magnetic stimulation of neural tissue," Nature communications, 3, p. 921.
- [2] Park, H. J., Bonmassar, G., Kaltenbach, J. A., Machado, A. G., Manzoor, N. F., and Gale, J. T., 2013, "Activation of the central nervous system induced by micro-magnetic stimulation," Nature communications, 4, p. 2463.
- [3] Rezai, A. R., Phillips, M., Baker, K. B., Sharan, A. D., Nyenhuis, J., Tkach, J., Henderson, J., and Shellock, F. G., 2004, "Neurostimulation system used for deep brain stimulation (DBS): MR safety issues and implications of failing to follow safety recommendations," Invest Radiol, 39(5), pp. 300-303.
- [4] Angelone, L. M., Potthast, A., Segonne, F., Iwaki, S., Belliveau, J. W., and Bonmassar, G., 2004, "Metallic electrodes and leads in simultaneous EEG-MRI: specific absorption rate (SAR) simulation studies," Bioelectromagnetics, 25(4), pp. 285-295.
- [5] Angelone, L., Ahveninen, J., Belliveau, J., and Bonmassar, G., 2010, "Analysis of the Role of Lead Resistivity in Specific Absorption Rate for Deep Brain Stimulator Leads at 3 T MRI," IEEE Trans Med Imaging, 29(4), pp. 1029-1038.
- [6] Seshan, K., 2012, Handbook of thin film deposition : techniques, processes, and technologies, Elsevier ; William Andrew, Amsterdam ; Boston Waltham.

- [7] Baker-Jarvis, J., Janezic, M., and DeGroot, D. C., 2010, "High-frequency dielectric measurements," *Instrumentation & Measurement Magazine, IEEE*, 13(2), pp. 24-31.
- [8] Polikov, V. S., Tresco, P. A., and Reichert, W. M., 2005, "Response of brain tissue to chronically implanted neural electrodes," *Journal of neuroscience methods*, 148(1), pp. 1-18.
- [9] Musa, S., Rand, D. R., Bartic, C., Eberle, W., Nuttin, B., and Borghs, G., 2011, "Coulometric Detection of Irreversible Electrochemical Reactions Occurring at Pt Microelectrodes Used for Neural Stimulation," *Analytical chemistry*, 83(11), pp. 4012-4022.
- [10] Chen, Y. S., Hung, Y. C., Liao, I., and Huang, G. S., 2009, "Assessment of the In Vivo Toxicity of Gold Nanoparticles," *Nanoscale Res Lett*, 4(8), pp. 858-864.
- [11] Lee, S. W., Seo, J.-M., Ha, S., Kim, E. T., Chung, H., and Kim, S. J., 2009 "Development of Microelectrode Arrays for Artificial Retinal Implants Using Liquid Crystal Polymers 10.1167/iavs.09-3743 " *Investigative ophthalmology & visual science*, 50 (12), pp. 5859-5866
- [12] Merrill, D. R., Bikson, M., and Jefferys, J. G., 2005, "Electrical stimulation of excitable tissue: design of efficacious and safe protocols," *Journal of neuroscience methods*, 141(2), pp. 171-198.
- [13] Ruohonen, J., Virtanen, J., and Ilmoniemi, R. J., 1997, "Coil optimization for magnetic brain stimulation," *Ann Biomed Eng*, 25(5), pp. 840-849.
- [14] Warman, E. N., Grill, W. M., and Durand, D., 1992, "Modeling the effects of electric fields on nerve fibers: determination of excitation thresholds," *IEEE transactions on bio-medical engineering*, 39(12), pp. 1244-1254.
- [15] Shuo, Y., Guizhi, X., Lei, W., and Qingxin, Y., 2012, "Analysis of Double Eight-Figure Coil for Transcranial Magnetic Stimulation Based on Realistic Head Model," *Electromagnetic Field Problems and Applications (ICEF)*, 2012 Sixth International Conference on, pp. 1-4.
- [16] Fleming, M. K., Sorinola, I. O., Newham, D. J., Roberts-Lewis, S. F., and Bergmann, J. H. M., 2012, "The Effect of Coil Type and Navigation on the Reliability of Transcranial Magnetic Stimulation," *Neural Systems and Rehabilitation Engineering, IEEE Transactions on*, 20(5), pp. 617-625.
- [17] Battocletti, J. H., Macias, M. Y., Pintar, F. A., Maiman, D. J., and Sutton, C. H., 2000, "A box coil for the stimulation of biological tissue and cells in vitro and in vivo by pulsed magnetic fields," *Biomedical Engineering, IEEE Transactions on*, 47(3), pp. 402-408.
- [18] Tao, P., Liang, L., Vanacken, J., and Herlach, F., 2008, "Efficient Design of Advanced Pulsed Magnets," *Applied Superconductivity, IEEE Transactions on*, 18(2), pp. 1509-1512.
- [19] Komae, A., and Shapiro, B., 2012, "Steering a Ferromagnetic Particle by Optimal Magnetic Feedback Control," *Control Systems Technology, IEEE Transactions on*, 20(4), pp. 1011-1024.
- [20] Grandori, F., and Ravazzani, P., 1991, "Magnetic stimulation of the motor cortex--theoretical considerations," *IEEE transactions on bio-medical engineering*, 38(2), pp. 180-191.
- [21] Long, J. R., and Copeland, M. A., 1997, "The modeling, characterization, and design of monolithic inductors for silicon RF IC's," *Solid-State Circuits, IEEE Journal of*, 32(3), pp. 357-369.

- [22] Tegopoulos, J. A., and Kriezis, E. E., 1985, Eddy currents in linear conducting media, Elsevier ; Distributors for the U.S. and Canada, Elsevier Science Pub. Co., Amsterdam ; New York New York, NY.
- [23] Yue, C. P., and Wong, S. S., 2000, "Physical modeling of spiral inductors on silicon," *Electron Devices, IEEE Transactions on*, 47(3), pp. 560-568.
- [24] Fox, C., 1987, *An introduction to the calculus of variations*, Dover Publications, New York.
- [25] Comsol, 2013, "Multiphysics, AC/DC Module User's Guide," Burlington, MA.
- [26] Barker, A. T., 1991, "An introduction to the basic principles of magnetic nerve stimulation," *Journal of clinical neurophysiology : official publication of the American Electroencephalographic Society*, 8(1), pp. 26-37.
- [27] Barker, A. T., Jalinous, R., and Freeston, I. L., 1985, "Non-invasive magnetic stimulation of human motor cortex," *Lancet*, 1(8437), pp. 1106-1107.
- [28] Eaton, H., 1992, "Electric field induced in a spherical volume conductor from arbitrary coils: application to magnetic stimulation and MEG," *Medical & biological engineering & computing*, 30(4), pp. 433-440.
- [29] Reilly, J. P., 1998, *Applied Bioelectricity : From Electrical Stimulation to Electropathology*, Springer Verlag.
- [30] Shawki, M. M., Elbelbesy, M. A., Shalaby, T. E., kotb, M. A., and Youssef, Y. S., 2010, "Studies On The Electric Field Distribution Using Different Electrode Shapes For Electrochemotherapy," *World Congress on Medical Physics and Biomedical Engineering*, September 7 - 12, 2009, Munich, Germany, O. D'Assel, and W. C. Schlegel, eds., Springer Berlin Heidelberg, pp. 252-255.
- [31] Ekstrom, L. B., Roelfsema, P. R., Arsenault, J. T., Kolster, H., and Vanduffel, W., 2009, "Modulation of the contrast response function by electrical microstimulation of the macaque frontal eye field," *J Neurosci*, 29(34), pp. 10683-10694.
- [32] Reilly, J. P., 1989, "Peripheral nerve stimulation by induced electric currents: exposure to time-varying magnetic fields," *Medical & biological engineering & computing*, 27(2), pp. 101-110.
- [33] Bonmassar, G., Freeman, D., Fried, S., and Gale, J., 2010, "Microscopic Magnetic Stimulation," *10th Vienna International Workshop on Functional Electrical Stimulation*, International FES Society, Vienna, Austria.
- [34] Bouchaud, J., Knoblich, B., and Wicht, H., 2006, "Will RF MEMS live up their promise?," *Microwave Conference, 2006. 36th European*, p. 1076.
- [35] Long, J., and Copeland, M., 1997, "The Modeling, Characterization, and Design of Monolithic Inductors for Silicon RF IC's," *IEEE JSSC*, 32(3), pp. 357-369.
- [36] Rosa, E., 1908, "The Self and Mutual Inductances of Linear Conductors," *Bulletin of the Bureau of Standards*, 4(2), pp. 301-344.
- [37] Guy, A., 1975, "Biophysics-energy absorption and distribution.," *AGARD Lecture Series, Radiation Hazards (Non-ionizing Radiations--Biological Effects and Safety Considerations*, 78.
- [38] NCRP, 1981, "Radiofrequency electromagnetic fields: properties, quantities and units, biophysical interaction, and measurement.," No. 67, National Council Radiation Protection and Measurements, Bethesda, MD.
- [39] Maxwell, J. C., 1954, *A treatise on electricity and magnetism*, Dover Publications, New York.
- [40] Grover, F. W., 2004, *Inductance calculations : working formulas and tables*, Dover Publications, Mineola, N.Y.
- [41] United States. National bureau of standards. [from old catalog], 1937, *Radio instruments and measurements*, U. S. Govt. print. off., Washington,.

- [42] Terman, F. E., 1943, Radio engineers' handbook, McGraw-Hill Book Company, inc., New York, London,.
- [43] Dwight, H. B., 1945, Electrical coils and conductors, their electrical characteristics and theory, McGraw-Hill book company, inc., New York, London,.
- [44] Roters, H. C., 1941, Electromagnetic devices, J. Wiley & sons Chapman & Hall, limited, New York, London,.
- [45] Smythe, W. R., 1967, Static and dynamic electricity, McGraw-Hill, New York,.
- [46] Montgomery, D. B., and Weggel, R. J., 1979, Solenoid magnet design : the magnetic and mechanical aspects of resistive and superconducting systems, R. E. Krieger Pub. Co., Huntington, N.Y.
- [47] Dill, H., 1964, "Designing Inductors for Thin Film Applications?," Electronic Design, pp. 52-59.
- [48] Rosa, E. B., and Grover, F. W., 1916, Formulas and tables for the calculation of mutual and self-inductance <revised>, Govt. print. off., Washington,.
- [49] Greenhouse, H., 1974, "Design of Planar Rectangular Microelectronic Inductors," Parts, Hybrids, and Packaging, IEEE Transactions on, 10(2), pp. 101-109.
- [50] Mohan, S. S., del Mar Hershenson, M., Boyd, S. P., and Lee, T. H., 1999, "Simple accurate expressions for planar spiral inductances," Solid-State Circuits, IEEE Journal of, 34(10), pp. 1419-1424.